X-651-73-156
PREPRINT

66289

MARS: MARINER 9 SPECTROSCOPIC EVIDENCE FOR H_2O ICE CLOUDS

(NASA-TM-X-66289) MARS: MARINER 9 SPECTROSCOPIC EVIDENCE FOR H2O ICE CLOUDS (NASA) 14 p HC $3.00 CSCL 04A

N73-27312

Unclas
G3/13 09148

ROBERT J. CURRAN
BARNEY J. CONRATH
RUDOLF A. HANEL
VIRGIL G. KUNDE
JOHN C. PEARL

JUNE 1973

GODDARD SPACE FLIGHT CENTER
GREENBELT, MARYLAND

X-651-73-156

PREPRINT

MARS: MARINER 9 SPECTROSCOPIC EVIDENCE FOR H_2O ICE CLOUDS

Robert J. Curran
Barney J. Conrath
Rudolf A. Hanel
Virgil G. Kunde
John C. Pearl

June 1973

GODDARD SPACE FLIGHT CENTER
Greenbelt, Maryland

MARS: MARINER 9 SPECTROSCOPIC EVIDENCE FOR H_2O ICE CLOUDS

Robert J. Curran, Barney J. Conrath, Rudolf A. Hanel,
Virgil G. Kunde and John C. Pearl

ABSTRACT

Spectral features observed with the Mariner 9 Interferometer Spectrometer are identified as those of water ice. Measured spectra are compared with theoretical calculations for the transfer of radiation through clouds of ice particles with variations in size distribution and integrated cloud mass. Comparisons with an observed spectrum from the Tharsis Ridge region indicate water ice clouds composed of particles with mean radius 2.0μm and integrated cloud mass $\lesssim 10^{-4}$ g cm^{-2}.

Ground-based observations indicate several distinct types of clouds occur in the Martian atmosphere including yellow clouds, assumed to be composed of blowing surface dust, and white clouds assumed to be condensed volatiles (1). White clouds have been observed to fall into two classes: 1) diffuse clouds with no particular aerographic location, and 2) discrete clouds at relatively fixed aerographic locations (2). Discrete clouds have been observed in the Nix Olympica - Tharsis Ridge area by Slipher (3), in the near-encounter pictures of Mariner 7 (4), and in the Mariner 9 orbital pictures (5). Although it has been suspected that the white clouds are composed of H_2O ice (6), no direct spectral evidence has previously been found. The present study presents spectroscopic data indicating the existence of H_2O ice clouds on Mars in the region of the shield volcanos of the Tharsis Ridge. Estimates are given for the cloud particle size and the integrated cloud mass.

Spectra of Mars have been obtained between 200 and 2000 cm^{-1} with a resolution of 2.4 cm^{-1} by the Infrared Interferometer Spectrometer (IRIS) carried by the Mariner 9 spacecraft. The observed spectral interval includes the molecular absorption features of both CO_2 and H_2O. Observations of these spectral features and their use in determining surface pressure, thermal structure, and water vapor amount have appeared in the literature (7). Broad absorption features, indicative of particulate (dust) absorption have also been observed during the Mariner 9 mission. Spectra obtained in the later part of the mission show additional broad absorption features which differ in position and width

from those of the dust clouds. These broad absorption features were found to correspond closely to those expected for H_2O ice clouds.

Fig. 1 compares spectra observed in the Tharsis Ridge region and the Lower Arcadia-Hougeria region with theoretical calculations for a water ice cloud. The spectrum measured over Lower Arcadia-Hougeria shows an approximately constant brightness temperature except for the CO_2 absorption band centered at 667 cm^{-1} and the rotational water vapor absorption lines below 400 cm^{-1}. In contrast the Tharsis Ridge spectrum exhibits a strikingly broad absorption feature extending from 550 to 950 cm^{-1} with a second broad absorption region evident between 225 and 350 cm^{-1}. Superimposed on the latter is a sharp spectral feature near 227 cm^{-1}. The theoretical ice cloud spectrum, described below, exhibits a similar behavior.

The IRIS fields of view for the two observed spectra are indicated in Fig. 2 by circles superimposed on a Mariner 9 television picture of the same region. Prominent in the picture are the summits of Nix Olympica and the three shield volcanoes along the Tharsis Ridge as well as the extensive cloud systems to the west of the volcanoes. Due to the substantial processing of the television data, information concerning the optical properties of the clouds cannot be inferred visually from Fig. 2. The cloud free spectrum is associated with the field of view in the left portion of the figure while the ice cloud spectrum from the field of view in the center of the figure includes the clouds off North and Middle spots. Since the summits of the volcanoes are visible in Fig. 2, the

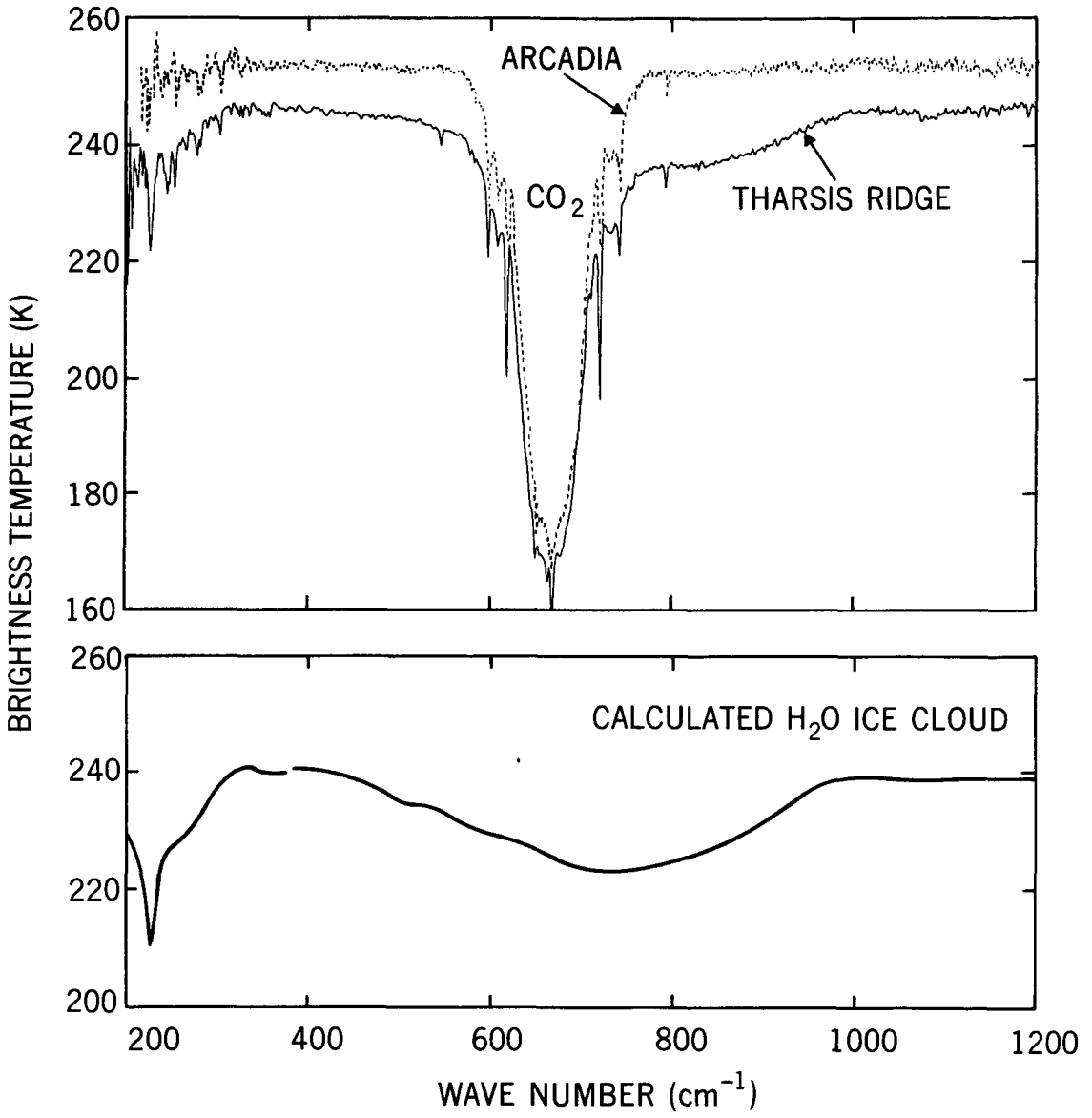

Figure 1. Mariner 9 IRIS measurements of the lower Arcadia-Hougeria region under clear conditions and of the Tharsis Ridge region under conditions of partial cloudiness. The Tharsis Ridge spectrum shows broad absorption features from 550-950 cm^{-1} and 225-350 cm^{-1}, similar to the theoretical ice cloud spectrum shown in the bottom portion of the Figure.

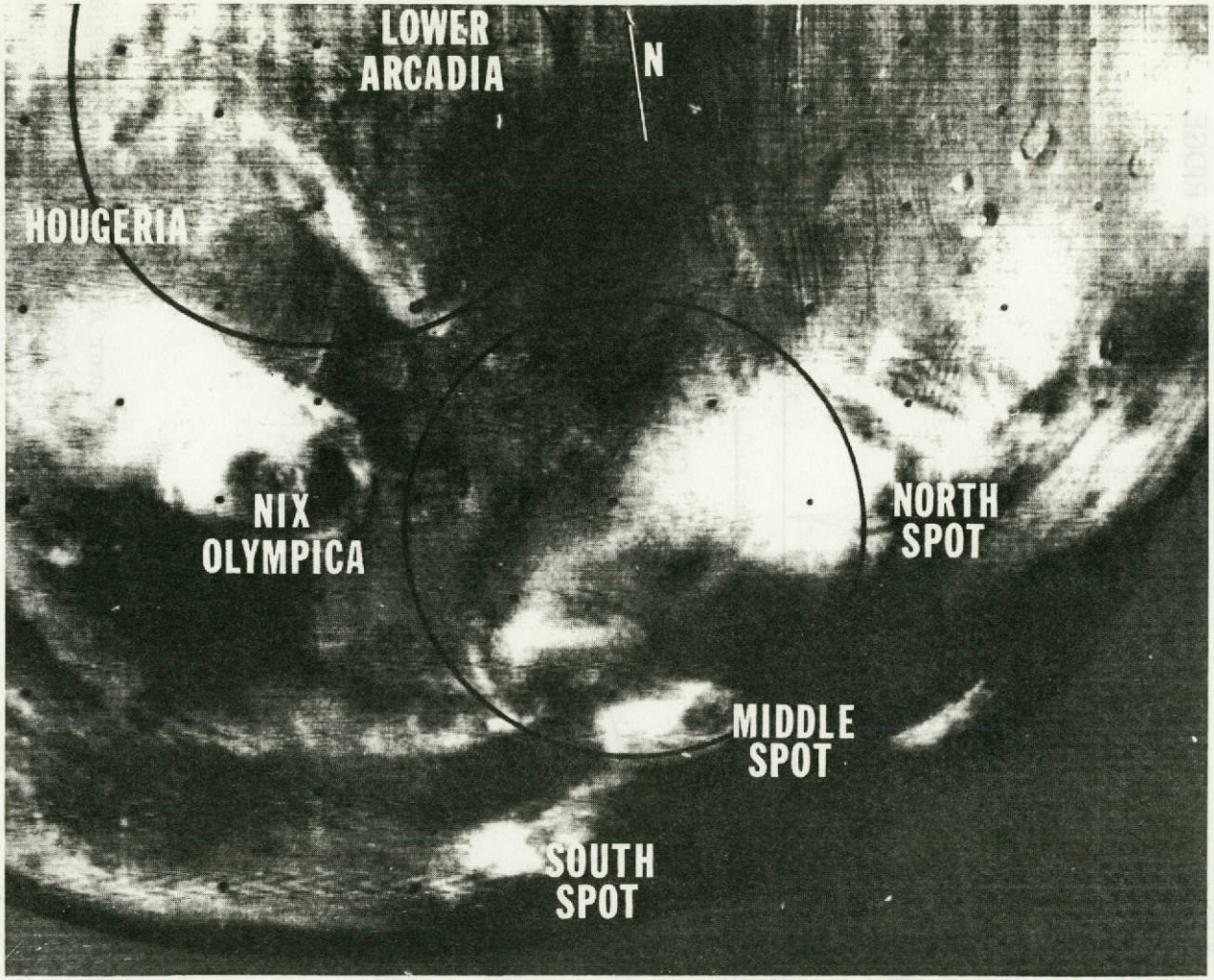

Figure 2. IRIS fields of view superimposed on a television photograph taken at nearly the same time as the spectral measurements. Indicated on the photograph are the summits of Nix Olympica and the three shield volcanoes along the Tharsis Ridge, North, Middle and South Spot.

bulk of the associated clouds must be near or slightly below these summits. It may be noted that the field of view is only partially filled by the clouds. Consequently, estimates of the number of particles in a vertical column as inferred from the measured infrared spectrum will be average values for the entire field of view.

The theoretical calculations are based on the theory of radiative transfer in a scattering atmosphere containing spherical particles with the refractive index of water ice. The transfer calculations include a numerical integration of the solution to the equation of radiative transfer over discrete atmospheric layers and over an angular mesh. The numerical integration is similar to that used by Herman, et.al. (8) for visible wavelengths. The complex refractive indices of water ice were used to calculate the absorption and scattering cross sections per unit volume and the angularly dependent phase matrix for a distribution of particle sizes. The assumed spherical shape appears to be a reasonable first approximation even for non-spherical particles when the wavelength of the radiation is much larger than the particle dimensions. This was found to be the case for the wavelengths and particle sizes encountered in the present study. The size distribution used for the calculations presented in Fig. 1 had a mean particle radius of 4 μm and fell to one tenth of its maximum value at 2.3μm and 5.7μm. Ice refractive indices for wavenumbers less than 380 cm^{-1} were obtained from Bertie, et al. (9) and those for wavenumbers greater than 380 cm^{-1} were obtained from recent measurements of Schaaf and Williams (10). The laboratory measurements of Bertie, et al. were performed using ice cooled to 77K while the measurements of Schaaf and

Williams were performed using ice cooled to 268K. The latter temperature more closely approximates Martian conditions. The use of two different sources for the refractive indices causes a small discontinuity in the calculated spectrum at 380 cm^{-1} The cloud temperature was chosen from the temperature distribution derived from the spectrum for the clear region; as the two spectra were obtained from the same general geographic area and at nearly the same time, it was assumed that the temperature profile from the clear spectrum was also applicable for the Tharsis Ridge spectrum. The summits of the great shield volcanoes extend very high into the atmosphere (11) and are generally situated between the 0.5 and the 1.0 mb pressure levels. The temperatures corresponding to these altitudes in the lower Arcadia - Hougeria region are 180 to 190 K. The top of the ice cloud was assumed to be slightly below the summit altitude at a temperature of 180 K and with a constant particle number density in a layer one kilometer thick. In addition to being sensitive to the cloud top temperature, the calculated spectra are dependent on the integrated cloud mass per unit area, which may be related to the visible optical thickness of the cloud, and on the mean radius of the particles. The results of theoretical calculations in the spectral interval 50 to 2000 cm^{-1} for ice clouds of different visible optical thicknesses are shown in Fig. 3a with the cloud particle size distribution having a mean equal to 4 μm. The corresponding integrated cloud mass per unit area and number of particles per unit area are shown in the inset. For each calculated spectrum the total number of particles in the cloud was adjusted to give the visible optical depth indicated. Increasing the

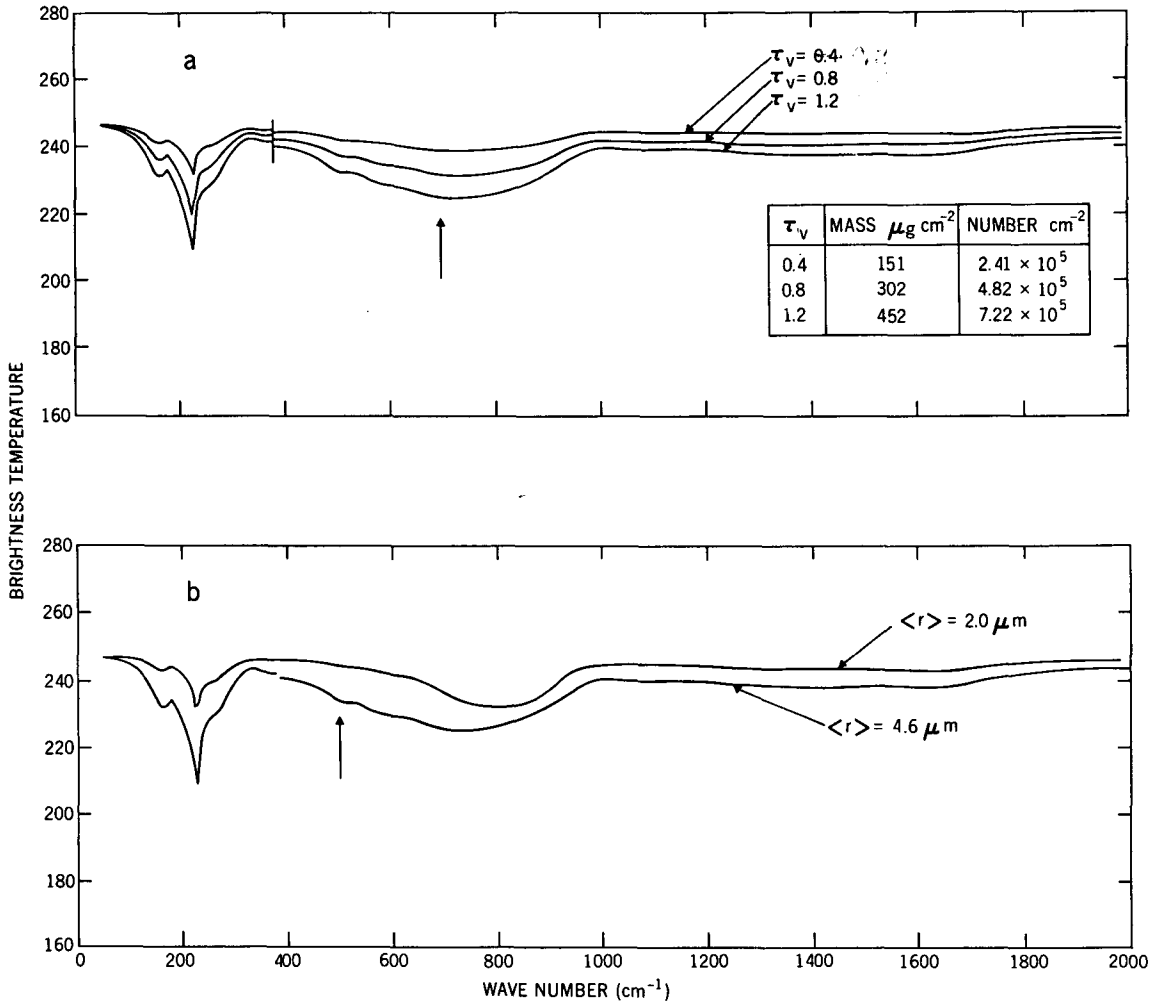

Figure 3. Results of calculations made for variations in cloud optical thickness (a) and in particle size distribution (b). The arrows indicate the position of greatest independent variation in brightness temperature with respect to each variable.

visible optical depth was found to strengthen the infrared attenuation throughout the spectrum and to preferentially strengthen the absorption features near 227 cm^{-1} and 750 cm^{-1}. Variation of the cloud top temperature produced an effect similar to variation of the cloud visible optical thickness. Therefore, it is not possible to uniquely determine both a cloud top temperature and visible optical thickness from the infrared spectral measurements alone.

The dependence of the emergent spectrum on the cloud particle size distribution may be characterized by a mean particle radius <r>. Fig. 3b shows spectra calculated for two different particle size distributions, assumed to be the modified gamma - distributions as discussed by Deirmendjian (12). The major effect of variation of the particle size distribution occurs near 500 cm^{-1} where the refractive indices of ice and the particle sizes encountered are such as to cause strong variation in the albedo for single scattering. The size distributions containing many large particles were found to have a larger albedo for single scattering near 500 cm^{-1} than distributions with relatively few large particles. Therefore, the particle size can be estimated by choosing that distribution which produces the best fit between measured and calculated spectra, especially near 500 cm^{-1}.

Since variation of the size distribution and variation of the visible optical thickness do not produce completely independent results it is necessary to match the measured and calculated spectra while varying both parameters. The best fit between the measured and calculated spectra was found for the mean radius <r> equal to 2 μm and the visible optical

depth equal to 0.8. The particle size distribution which produced the best fit to the measured spectrum was the cloud C.3 distribution of Diermendjian (12). This particle size distribution falls to one tenth of its maximum value at particle radii 1.2 μm and 2.8 μm. From the best fit visible optical thickness the integrated mass of the cloud was found to be 0.5×10^{-4} g cm^{-2}. This value can be contrasted with the integrated water vapor amount of 5×10^{-3} g cm^{-2} found in the near-by lower Arcadia-Hougeria spectrum. The source of the water forming the observed clouds is unknown. Discussion of the evidence supporting either local degassing from the surface or orographic uplift coupled with convection is presented by Leovy, Briggs and Smith (5).

Many spectra collected by the Mariner 9 IRIS contain spectral features indicative of H_2O ice. However, the Tharsis Ridge spectrum has been chosen because of its historical significance and because its strong thermal contrast favors quantitative interpretation of the ice features. The inferred mean particle size has been found to be consistent with studies of ice crystal development at very cold temperatures and low pressures.

References and Notes

1. G. de Vaucouleurs, Physics of the Planet Mars (Faber and Faber Limited London, 1961), pp 77-98.

2. S. A. Smith and B. A. Smith, ICARUS. 16, 509 (1972).

3. E. C. Slipher, The Photographic Story of Mars (Sky Publishing Corporation, Cambridge, Mass, 1962), pp 27-36.

4. C. B. Leovy, J. GEOPHYS, RES. 76, 297 (1971).

5. C. B. Leovy, G. A. Briggs and B. A. Smith, J. GEOPHYS. RES., in press.

6. A. Dollfus, Annales d'ASTROPHYSIQUE. SUP. NO. 4, 114 (1957).

7. R. A. Hanel, B. J. Conrath, W. A. Hovis, V. G. Kunde, P. D. Lowman, J. C. Pearl, C. Prabahakara, B. Schlachman and G. V. Levin, SCIENCE 175, 305(1972); R. A. Hanel, B. J. Conrath, W. A. Hovis, V. G. Kunde, P. D. Lowman, W. C. Maguire, J. C. Pearl, J. S. Pirraglia, C. Prabhakara, B. Schlachman, G. Levin, P. Straat, and T. Burke, ICARUS 17, 423(1972); B. J. Conrath, R. J. Curran, R. A. Hanel, V. G. Kunde, W. C. Maguire, J. C. Pearl, J. A. Pirraglia, J. E. Welker, and T. Burke, J. GEOPHYS. RES., in press.

8. B. M. Herman and S. R. Browning, J. ATMOS. SCI. 22, 559 (1965).

9. J. E. Bertie, H. J. Labb, and E. Whalley, J. CHEM. PHYS. 50, 4501 (1969).

10. J. W. Schaaf and D. Williams, J. OPT. SOC. AM. in press.

11. C. W. Hord, C. A. Barth, A. I. Stewart, A. L. Lane, ICARUS 17, 443(1972); K. R. Blasius, J. GEOPHYS, RES., in press; A. J. Kliore, G. Fjeldbo, B. L. Seidel, M. J. Sykes; and P. M. Woiceshyn, J. GEOPHYS. RES., in press; S. S. C. Wu, F. J. Shafer, G. M. Nakata, R. Jordan, and K. R. Blasius, J. GEOPHYS. RES., in press.

12. D. Deirmendjian, Electromagnetic Scattering on Spherical Polydispersions (American Elsevier Publishing Company, Inc., New York, 1969), pp 77-83.